A simple and robust method to calculate the shear deformation of RC beams and columns.

Hernández-Montes E. and Gil-Martín L.M.

Nomenclature

$A_{c,eff}$	effective area of concrete, perpendicular to the bar, at a distance from the bar smaller than $7.5d_b$
$A_{c,eff,min}$	minimum effective area of concrete, perpendicular to the bar, at a distance from the bar smaller than 7.5ϕ, with ϕ as the diameter of the bar for the minimum amount required
A_s	Area of steel
A_{sv}	Area of the vertical steel.
A_ϕ	Area of the vertical leg
b_w	breadth of the web
d	effective depth
d_b, ϕ	bar diameter in mm.
E_{cm}	Secant modulus of elasticity of concrete
E_s	Modulus of elasticity of reinforcing steel
f_{ctm}	mean concrete strength in tension
f_y	steel yield stress
f_{vy}	yield stress of the transverse steel reinforcement
n_l	number of legs for stirrup
s	distance between vertical bars
z	lever arm

ε_{ay}	mean strain for apparent yield
ε_c	concrete strain
ε_{mean}	mean strain
ε_s, ε_{sv}	steel strain, steel strain of the vertical bar
ε_1	strain in the principal direction of tension

γ	shear rotation
σ_{ct}	concrete stress in tension
σ_s	steel stress
σ_{sv}	stress of vertical steel
σ_1	concrete tensional stress in the principal direction of tension
τ_{ci}	shear stress in the crack
θ	crack angle

Abstract

This paper presents a simple and robust method for calculating the shear deformation, up to collapse, of reinforced concrete beams and columns. The method is based on the fundaments of the shear deformation of reinforced concrete elements. A conceptual review of the different

models used to describe the tension stiffening of concrete is also presented. A detailed example is shown.

1. Introduction

In general, Reinforced Concrete (RC) codes, such as Eurocode 2[1] or ACI-318[2] do not take into account shear deformation, being the above obvious assumption for structural engineers. Nevertheless, the earthquake engineering community is concerned about the need for an efficient fiber beam-column element that considers flexure and shear interaction ([3], [4], [5],[6],[7]). This is due to the fact that the shear collapse of beams and columns under seismic actions is of great importance, see Fig.1.

Figure 1. Shear deformation of columns during the Lorca earthquake (2011), adapted from [8].

In the search for a fiber beam-column element that considers flexure and shear, different models of concrete have been used. Usually, the most popular ones are the Mander model for confined concrete [9] and the MCFT (Modified Compression Field Theory) [10] or the RA-STM (Rotating Angle Softened Truss Model) [11] for concrete tension stiffening.

The main discrepancy between the MCFT and RA-STM concerns the steel bar model: while the MCFT uses a bare bar model, the RA-STM considers an embedded bar model. In an effort to show the equivalence of both theories, an interesting refinement of the original MCFT formulation was done in [12]. Both the MCFT and the RA-STM describe the tension stiffening of concrete using several functions. These functions need conditional checks to define their ranges of applicability (an apparent yield check in the case of the RA-STM and a crack check in the case of the MCFT). In both theories, the tension stiffening effect is considered to exist even for an average strain greater than the steel yield strain, an assumption which is also supported by other authors [13]. On the contrary, well recognized structural software packages such as [14] or [15] consider linear approximations for the tension stiffening response of concrete, assuming that for strain values beyond the steel yield strain, tension stiffening disappears. The above assumption is supported by authors such as (e.g. [16]).

This work uses a bilinear approximation for the description of tension stiffening behavior, in such a way that the apparent yield and yielding of steel coincide. In doing so, the need for a

distinction between bare bar and embedded bar models is no longer necessary. A conceptual review of the tension stiffening models is summarized in Appendix A. Regarding the steel model, the Eurocode 2[1] bilinear steel model with strain hardening is used here. Additionally, for the case of B-Regions, the authors have considered that the angle of cracks can be deduced from linear elastic theory. Therefore, for beams with no axial force, cracks at an angle of 45º are considered.

Taking all of this information into account, a procedure to calculate the shear deformation of RC beams and columns is presented in this paper.

2. Bilinear tension stiffening model

In this work, a bilinear tension stiffening model is proposed, see Fig.2. The descending branch is defined by a certain point ψf_{ctm} ($\psi \leq 1$) of the ascending branch and the point corresponding to the steel yield strain (ε_y), for which the tension stiffness capacity is zero. Additionally, the model adopted presents a residual plateau, formulated using [13]. Because the model adopted lacks an apparent yield, a bare bar model is considered (see Appendix).

The authors propose this tension stiffening model for two reasons: to obtain a computationally robust method, and to choose ψ so that the capacity of the effective area of concrete in tension equals the capacity of the minimum transversal steel area required by code. The later condition ensures that the branch D-E in Fig. A.7 is always ascending. Note that current provisions set a minimum amount of transverse steel to avoid sudden failures.

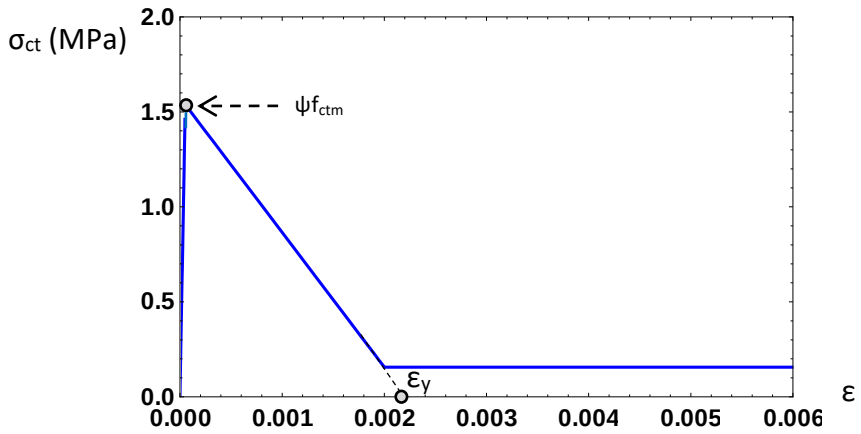

Figure 2. Bilinear model for tension stiffening.

3. Compatibility and equilibrium equations

Compression Field Theories [17] provide answers to the problem of shear and bending interaction using a continuum mechanics formulation. They have greatly helped with the understanding of the deformation of RC elements. In these theories, the equilibrium and compatibility equations can be formulated at a cross-sectional level or at a fiber level.

In the procedure proposed, for the sake of robustness, the only equilibrium equation considered is the one corresponding to the vertical equilibrium. Crack angles are obtained from continuum

elastic mechanics, (i.e. 45º for RC beams and 0.5ArcTan(2τ/σ) for columns [18]) which is quite close to reality in B-Regions due to the fact that the formation of secondary cracks is highly unlikely [19]. Without any loss of generality, only shear reinforcement which is perpendicular to the axis of the element is considered in this work, see Fig. 3. V_{Ed} is the shear demand, defined by the exterior action and by the geometry of the element (see the example in the next section).

Each one of the legs of the stirrups will contribute to the shear response according to the force-strain relation given in Eq.(1) (see Fig. 3) with $A_{c,eff}$ as the effective area associated to each leg and ε the longitudinal strain of the leg of the stirrup:

$$A_{\phi}\sigma_{sv}(\varepsilon)+A_{c,eff}\sigma_{ct}(\varepsilon) \tag{1}$$

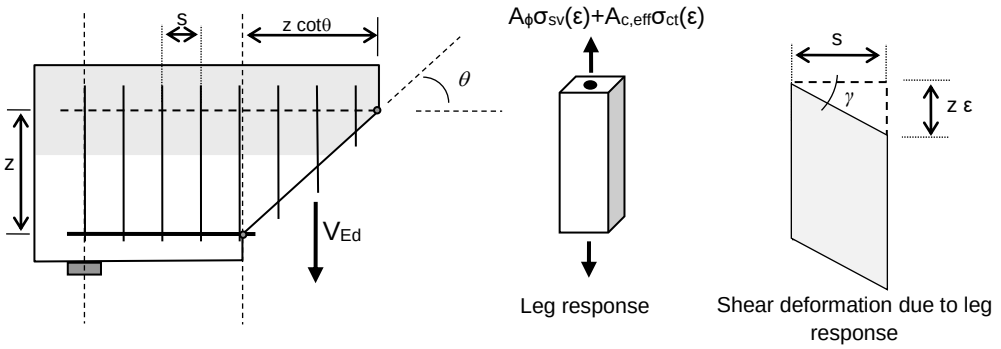

Figure 3. Vertical equilibrium and shear deformation

The deflection due to shear consists of the sliding of an adjacent cross sections of the beam, see Fig.3. In our case, two cross-sections separated by a distance *s* (distance between vertical bars) have been considered and so the sliding is directly deduced from the deformation of the legs as:

$$\gamma=\frac{dy}{dx}=\frac{\varepsilon z}{s}\rightarrow\varepsilon=\frac{\gamma s}{z} \tag{2}$$

where *y* is the deflection due to the shear deformation, *x* is the coordinate along the axis of the element, *z* is the lever arm and *γ* is the shear rotation.

Imposing vertical equilibrium and accounting for Eq.1 and Eq. 2:

$$V_{Ed}(x)=\frac{z\,Cot(\theta)}{s}n_l\left(A_{\phi}\sigma_{sv}\left(\frac{\gamma s}{z}\right)+A_{c,eff}\sigma_{ct}\left(\frac{\gamma s}{z}\right)\right) \tag{3}$$

with n_l as the number of legs on each stirrup.

The value of *γ* as a function of *x* (i.e. *γ(x)*) can be obtained from Eq. (3) and therefore, the shear deformation can be determined by the numerical integration of *γ(x)* along the length of the beam. The authors have used finite differences to do it, and the code developed is available on request. For the sake of simplicity, in this piece of work we have used *Δx=s*.

Example

The example shown in Fig.4 has been adapted from [20]. The values of the effective depth, the secant modulus of elasticity of concrete and steel yield stress are: d=450 mm, E_{cm}=30500 MPa and f_y=400 MPa, respectively.

In the original example, the beam was subjected to a uniform load *q* equal to 16.9 kN/m. For this load, the maximum deflection calculated according to ACI-318[2] is 10.7 mm while the value of the maximum deflection calculated using the simplified method of EC2[1] (i.e. interpolating deflections and considering shrinkage) is 11.2 mm.

The elastic modulus of steel is E_s=200000 MPa, the plastic modulus considered here is E_s/100 and the maximum strain is 0.01. It is also assumed that the crack angle is 45º.

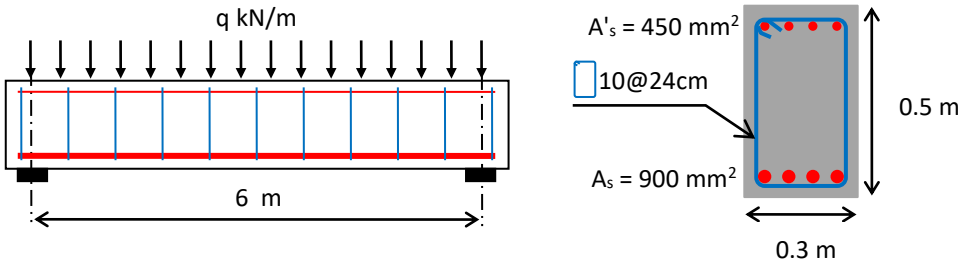

Figure. 4. Example of reinforced concrete beam.

The shear demand V_{Ed} is calculated as a function of *q*. For q=16.9 kN/m V_{Ed} is shown in Fig. 5. At a distance of less than *d* from the face of the support, the shear demand remains constant (EC2 [1], §6.2.1(8)).

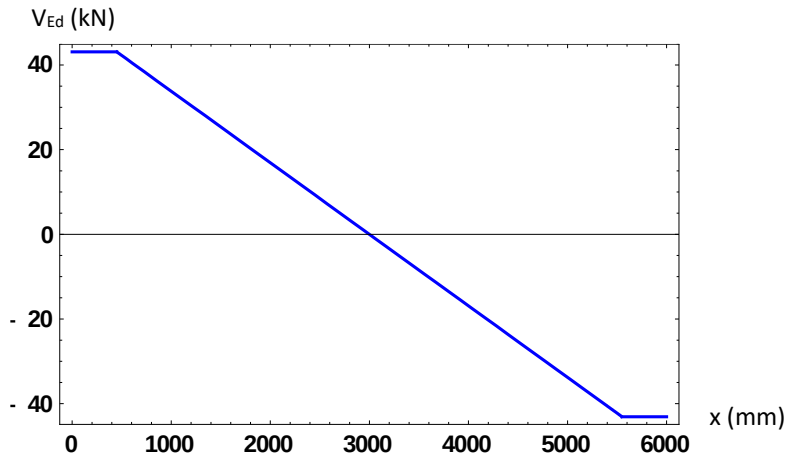

Figure 5. Shear demand in the beam in Fig. 4 for q=16.9 kN/m.

The components of the right side of Eq. 3 and their summation are shown in Fig.6 for the example studied. The dashed line is the contribution of the steel. The thin line corresponds to the contribution of concrete in tension (tension stiffening), assuming a tension stiffening bilinear model defined by ψ=0.6 (see Fig. 2). This value of ψ is deduced from the minimum shear

reinforcement ratio proposed by EC2[1] (Expression 9.5N of EC2) that applied to this beam lead to:

$$\frac{n_l A_\phi}{s\, b_w} = 0.08 \frac{\sqrt{f_{ck}}}{f_y} \rightarrow \phi = 6.8\, mm$$

$$\psi\, f_{ctm} A_{c,eff\ min} = \psi\, f_{ctm}(50 + 7.5\phi)(2{\cdot}7.5\phi) = \frac{\pi \phi^2}{4} f_y \rightarrow \psi = 0.6$$

The bold line is the summation of both contributions.

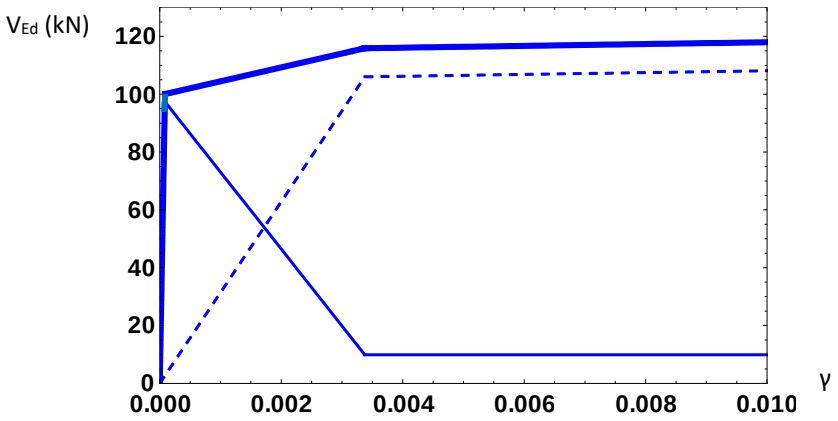

Figure 6. Shear response as a function of the shear rotation

Shear rotation and shear deflection for values of *q* ranging from 17 to 47 kN/m have been represented in Fig.7 (in this example, collapse happens at q=47.1 kN/m). It can be observed that the response is in the linear elastic range of up to q=39 kN/m (Fig. 7a). For q=17 kN/m, the shear deformation (=0.06mm) is negligible in comparison with the bending deformation (=11mm). For q=39 kN/m, the maximum deformation due to shear is 0.15 mm at mid span, see Fig. 7a.

For load values above q=39 kN/m, a drastic increment of both the shear rotation and the shear deflection happens in the vicinity of the supports, see Figs. 7b and 7c. This increment is associated to the yielding of the legs of the stirrups.

As can be observed in Fig. 7, the maximum shear deflection at mid span for q=40 kN/m is 0.35 mm, while for q=47 kN/m, it is 9.02 mm. The load increase and its corresponding deflection increase show a ductile behavior appropriate for seismic engineering design.

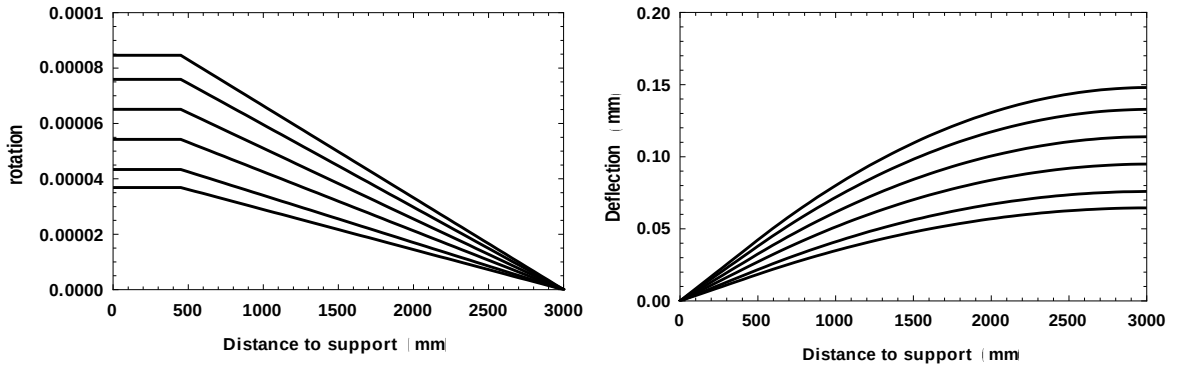

a) Shear rotation and shear deflection for q= 17, 20, 25, 30, 35, 38 y 39 kN/m

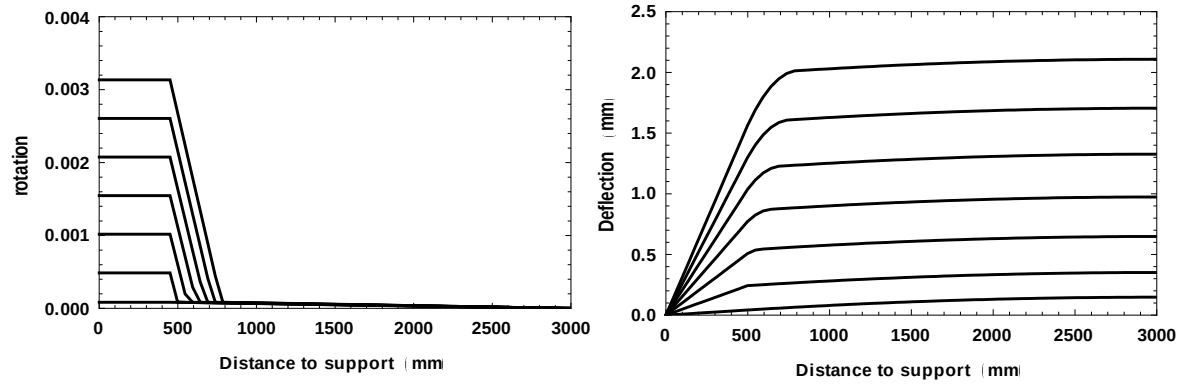

b) Shear rotation and shear deflection for q= 39, 40, 41, 42, 43 y 45 kN/m

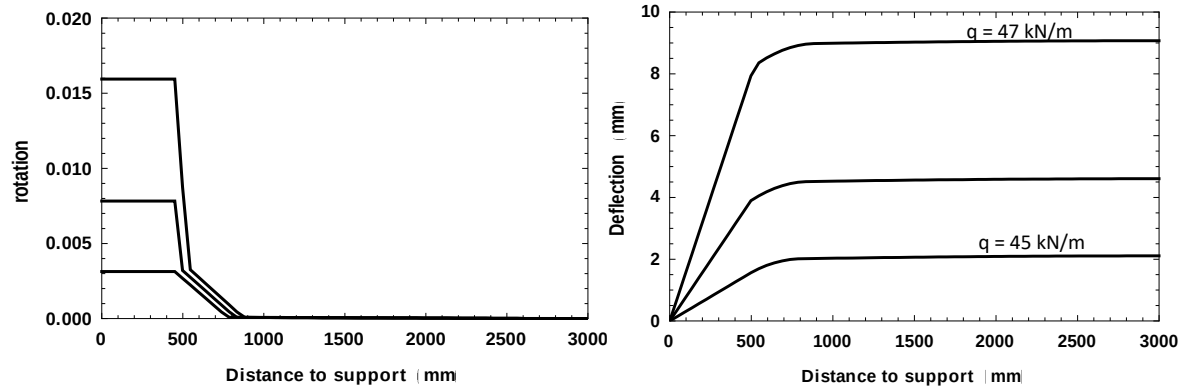

c) Shear rotation and shear deflection for q= 45, 46, y 47 kN/m

Figure 7. Shear rotation and shear deflection in the beam.

Conclusions

In this paper, a simple procedure to calculate the shear deflection of reinforced beams and columns is presented. The procedure is easy to implement with computer software. The methodology is applicable to the complete range of loadings and it is very interesting for the detection of shear collapse. The main advantages of the method proposed are its robustness and simplicity. An example has been studied to demonstrate the utility of the procedure proposed.

Appendix A. The steel models for tension stiffening of concrete: bare bar versus embedded bar.

Tension stiffening of concrete is the ability of concrete to withstand stresses after cracking. This is due to the presence of reinforcing steel. A good expression of this property is given by [12] (Eq. A.1). As mentioned in the Introduction Section, this was proposed in an attempt to unify the results of both the MCFT and the RA-STM:

$$\sigma_{ct}(\varepsilon_c) = \frac{f_{ctm}}{1+\sqrt{3.6M\varepsilon_c}} \quad where \quad M = \frac{A_{c,eff}}{\sum d_b \pi} \; values\ in\ mm \tag{A.1}$$

Eq. A.1 and the experimental results obtained using [16] are plotted together in Fig. A.1. See [16] for the sizes and properties of the experiments. It can be observed that for strain values greater than 0.002 (the yield strain of steel in this case) the stresses are negligible in the experimental results.

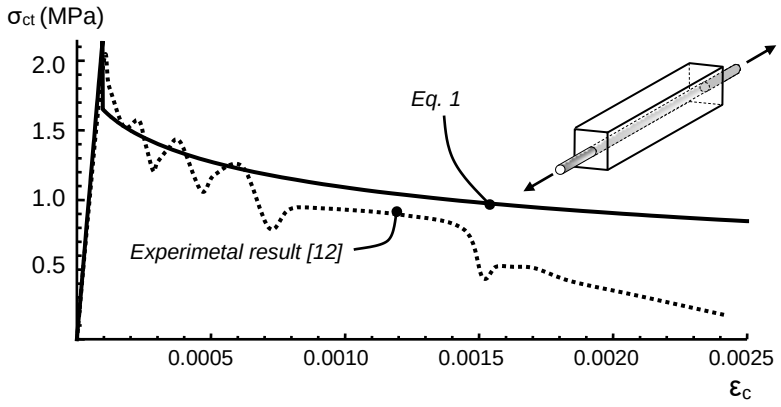

Figure A.1. Tension stiffening of concrete.

The MCFT considers a bare bar model, which can be modeled as bilinear with no strain hardening, see the blue curve in Fig. A.2, where ε_y is the yield strain. On the contrary, other theories use embedded bar models ([11],[21]), the red curve in Fig. A.2. As can be seen in Fig. A.2, the embedded bar model separates from the bare bar model at the apparent yield strain: ε_{ay}.

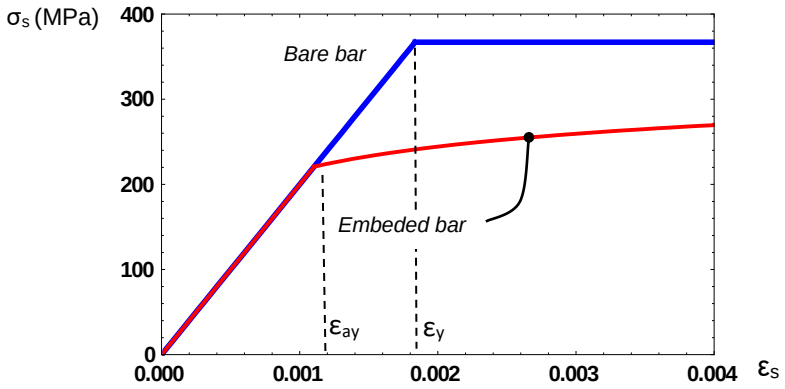

Figure A.2. Example of bare bar model in blue and embedded bar model in red.

Figure A.3 and Eq. (A.2) show the equilibrium of forces between a crack section and a mean section of an embedded bar subjected to tension, assuming that the steel is yielding at the crack:

$$\underbrace{A_s f_y}_{crack\ section} = \underbrace{A_s \sigma_s(\varepsilon_{mean}) + A_{c,eff}\sigma_{ct}(\varepsilon_{mean})}_{mean\ section} \qquad (A.2)$$

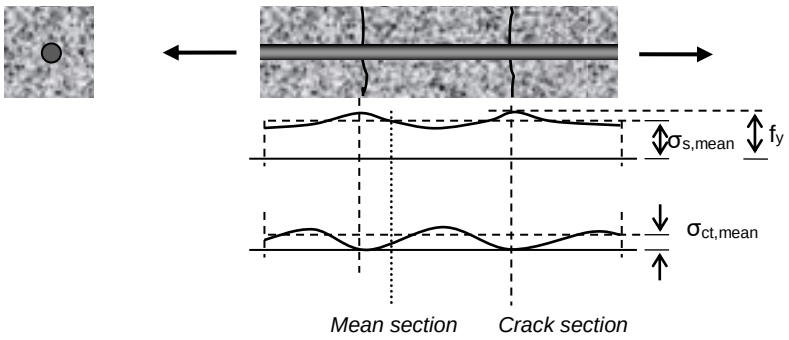

Figure A.3. Embedded bar in tension. The steel stress at the crack is the steel yield stress, f_y.

Example

Figure A.4 shows the components of Eq.A.2 for a leg of the stirrups of the classic example developed on page 352 of [17]. With ϕ=9.5 mm, A_{ceff}=76×152 mm^2, f_{ctm}=2MPa and f_y=367 MPa (f_{ck}=38.6 MPa, f_{cm}=46.6 MPa, E_{cm}=34909 MPa). The red curve represents the tension stiffening force according to Eq.(A.1) with $A_{c,eff}$ as the concrete area affected. The blue curve shows the behavior of the bare bar. The term on the left side of Eq.(A.2) is the tension capacity of the bare bar (=26 kN), which corresponds to the maximum value of the summation of both terms at the right side of Eq.(A.2) (see brown curve in Fig. A.4).The result of this is:

- The mean strain of the element when the first yield of the steel happens at the crack (which is also known as "apparent yield" (ε_{ay})) can be obtained by solving Eq. (A.2) for $\varepsilon_{mean} = \varepsilon_{ay}$. In this case ε_{ay}=0.0011.

- Eq.(A.2) provides a formulation for the embedded bar, based on the tension stiffening model for strain values greater than the apparent yield strain. See Eq.(A.3) and the yellow curve in Fig.A.4.

$$\begin{aligned} \sigma_s &= f_y - \frac{A_{c,eff}}{A_s}\sigma_{ct}(\varepsilon) \quad if \quad \varepsilon_s \geq \varepsilon_{ay} \\ \sigma_s &= E_s\varepsilon_s \qquad\qquad\qquad if \quad \varepsilon_s < \varepsilon_{ay} \end{aligned} \qquad (A.3)$$

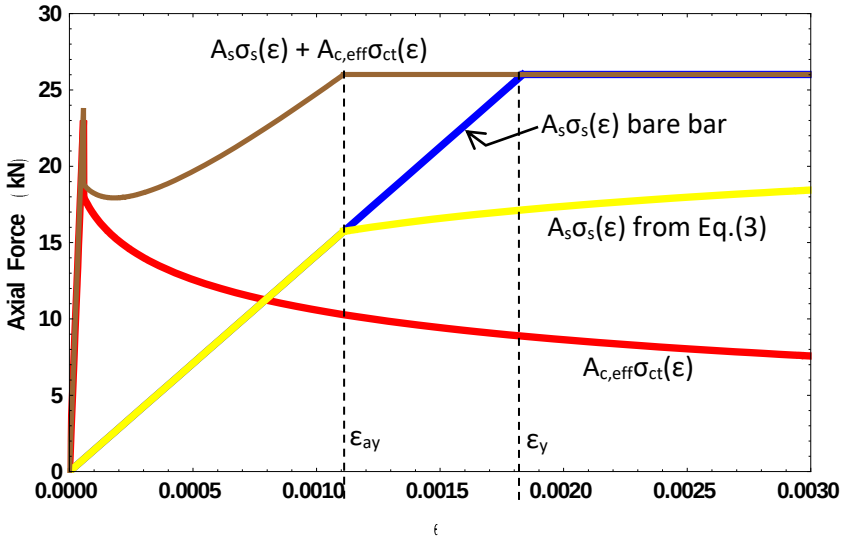

Figure A.4. Tension stiffening force versus strain for the example in page 352 of [17].

As can be seen in Fig.A.1, the values of tension stiffening given by Eq.(A.1) differ from experiments for strains greater than 0.0006. Therefore, Eqs (A.1) and (A.3) do not provide good results and they need to be adjusted for strain values greater than a certain value (e.g. 0.0006 in Fig. A.1). In fact, some authors claim that for strain values greater than the yield strain of steel (ε_y ~ 0.002), tension stiffening disappears [16]. The RA-STM solves this problem by introducing a new embedded bar model that is not based on the formulation of the concrete in tension, as in Eq.(A.3). In doing so, the tension stiffening phenomenon is modeled in the RA-STM with two different functions which are not connected by equilibrium: one for the concrete and another one for the embedded bar. Alternatively, the MCFT solves the problem by introducing a shear stress parallel to the crack (known as "crack check"), and so tension stiffening is defined in two domains while keeping the bare bar model for the reinforcing steel. For the crack check, the MCFT imposes the equilibrium in the principal direction of tension, see Fig. A.5. It is important to notice that the compression field theories apply the stress-strain relations exclusively in principal directions and assume that the principal directions of both strains and stresses coincide.

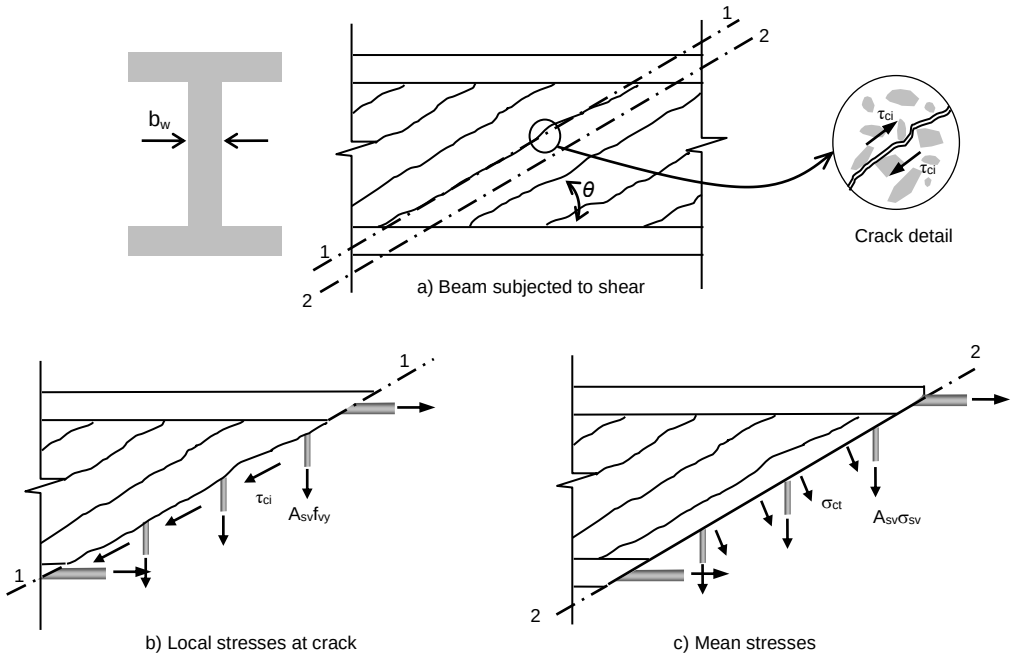

Figure A.5. Crack check according to MCFT. Adapted from [17].

According to the "crack check", the resultant vertical force in the crack (when the steel is yielding) and between the cracks has to be equivalent (see page 349 of [17]):

$$A_{sv}\sigma_{sv}\left(\frac{z}{s\tan\theta}\right)+\sigma_{ct}\frac{b_w z}{\tan\theta}=A_{sv}f_{vy}\left(\frac{z}{s\tan\theta}\right)+\tau_{ci}b_w z \tag{A.4}$$

Eq.(A.4) is presented as a limitation to σ_{ct} (i.e. to the tension stiffening of concrete) introducing a new function: the shear stress at the crack parallel to the crack (τ_{ci}), see [17]. Following this way of thinking, the refined tension curve of concrete according to the MCFT could be expressed as:

$$\sigma_1(\varepsilon_1)=Min\begin{cases}\sigma_{ct}(\varepsilon_1)\\ \tau_{ci}(\varepsilon_1)\tan\theta+\dfrac{A_{sv}}{sb_w}\left(f_{vy}-\sigma_{sv}(\varepsilon_v)\right)\end{cases} \tag{A.5}$$

where σ_{sv} is the stress of the transverse steel considering the bare bar model shown in blue in Fig. A.2 and f_{vy} is the yield stress of the transverse steel reinforcement.

Eq.(A.5) is coupled with other equations and it has to be solved simultaneously with both compatibility and equilibrium equations, see [17], [18].

Example -continuation-

Fig. A.6 shows the tension stiffening of concrete (σ_1-ε_1) curve obtained from Eq. (A.5) for the example considered above.

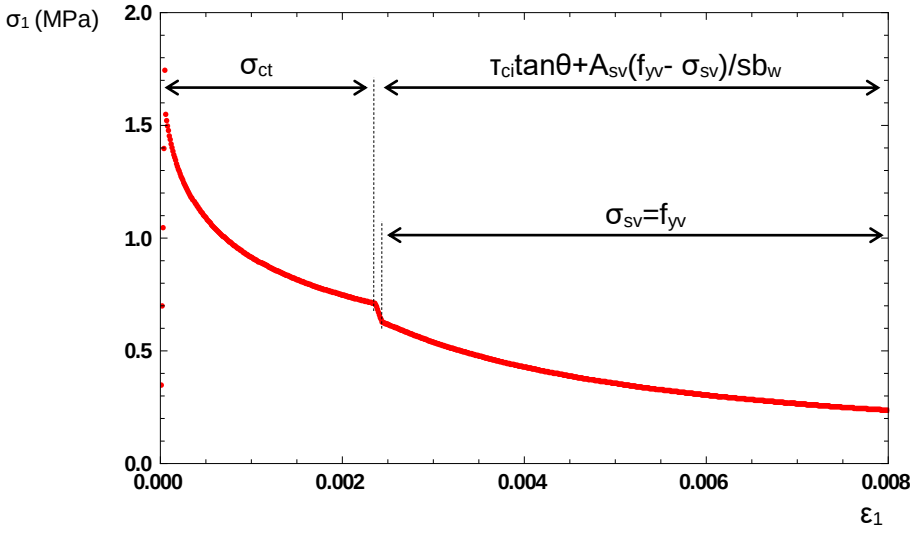

Figure A.6. σ_1-ε_1 curve for the example developed in [17], page 352.

It is interesting to notice that Eq.(A.4) can be interpreted in a similar way as Eq.(A.2).

Let us assume that σ_{ct} is already known from using Eq.(A.1) and then Eq.(A.4) is solved using σ_{sv}. In doing so, σ_{sv} could be a new formulation for an embedded bar model, but instead of this interpretation, the authors of the MCFT chose to see it as a corrected formulation of σ_{ct}. It can be concluded that both embedded and bare bar models constitute equivalent interpretations of an equilibrium equation. In other words, the strong decay of the tension stiffening beyond the apparent yield strain is solved by the MCFT by introducing the crack shear stress, while the RA-STM introduces the embedded steel model.

In order to match experimental results while keeping Eq.(A.3) valid, [21] modified the effective area (A_{ceff}) by multiplying it by a degradation coefficient, which is another alternative to the RA-STM and MCFT approaches. In [21] it was proved that the value of this coefficient decreases as the strain level increases, with 0.3 as a good constant approximation for strain values beyond apparent yield strain.

As previously mentioned, software programs such as [14] or [15] use linear models to simulate the behavior of concrete in tension. In these cases, if the tension stiffening model adopted is such that the summation of the contribution of the bare bar plus the contribution of concrete is always smaller than the capacity of the steel, then the apparent yield strain will coincide with the yield strain. See Fig. A.7 for the example analyzed in this Appendix.

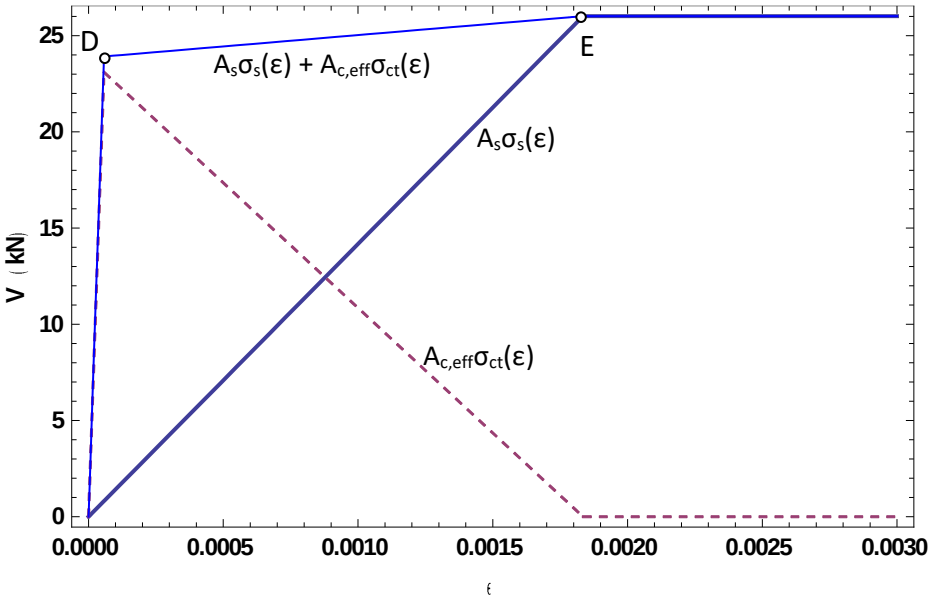

Figure A.7. Absence of apparent yield in linear model of tension stiffening

All the compression field theories [10], [11], [21] present a residual tension stiffening capacity. Bond-slip and tension stiffening are holistically related, [22] showed that the plateau presented in the residual bond is related to the clear spacing between reinforcement ribs. The value of the residual tension stiffening capacity used in this work was the one deduced in [13].

References

[1] CEN, "CEN. Eurocode 2: design of concrete structures — Part 1-1: general rules and rules for buildings. European Committee for Standardization." p. 225, 2004.

[2] ACI, "ACI 318 (2019). Building code requirements for structural concrete and commentary, American Concrete Institute; Farmington Hills, MI, USA." .

[3] D.-C. Feng and J. Xu, "An efficient fiber beam-column element considering flexure–shear interaction and anchorage bond-slip effect for cyclic analysis of RC structures," *Bull. Earthq. Eng.*, vol. 16, no. 11, pp. 5425–5452, 2018, doi: 10.1007/s10518-018-0392-y.

[4] P. Ceresa, L. Petrini, R. Pinho, and R. Sousa, "A fibre flexure-shear model for seismic analysis of RC-framed structures," *Earthq. Eng. Struct. Dyn.*, vol. 38, no. 5, pp. 565–586, Apr. 2009, doi: 10.1002/eqe.894.

[5] Z. Huang, Y. Tu, S. Meng, U. Ohlsson, B. Täljsten, and L. Elfgren, "A practical method for predicting shear deformation of reinforced concrete beams," *Eng. Struct.*, vol. 206, no. June 2018, p. 110116, 2020, doi: 10.1016/j.engstruct.2019.110116.

[6] Z. L. Du, Z. X. Ding, Y. P. Liu, and S. L. Chan, "Advanced flexibility-based beam-column element allowing for shear deformation and initial imperfection for direct analysis," *Eng. Struct.*, vol. 199, no. August, p. 109586, 2019, doi: 10.1016/j.engstruct.2019.109586.

[7] Z. Huang, Y. Tu, S. Meng, C. Sabau, C. Popescu, and G. Sas, “Experimental study on shear deformation of reinforced concrete beams using digital image correlation,” *Eng. Struct.*, vol. 181, no. June 2018, pp. 670–698, 2019, doi: 10.1016/j.engstruct.2018.12.056.

[8] L. Hermanns, A. Fraile, E. Alarcón, and R. Álvarez, “Performance of buildings with masonry infill walls during the 2011 Lorca earthquake,” *Bull. Earthq. Eng.*, vol. 12, no. 5, pp. 1977–1997, 2014, doi: 10.1007/s10518-013-9499-3.

[9] J. Mander, M. Priestley, and R. Park, “Theoretical stress-strain model for confined concrete,” *J. Struct. Eng.*, vol. 114, no. 8, pp. 1804–1826, 1988.

[10] F. J. Vecchio and M. P. Collins, “The Modified compression-Field Theory for RC Elements Subjected to Shear,” *ACI J.*, vol. 83, no. 22, pp. 219–231, 1986.

[11] T. Hsu, “Softened truss model theory for shear and torsion,” *ACI Struct. J.*, vol. 85, no. 6, pp. 624–635, 1988.

[12] E. C. Bentz, “Explaining the riddle of tension stiffening models for shear panel experiments,” *J. Struct. Eng.*, vol. 131, no. 9, pp. 1422–1425, Sep. 2005, doi: 10.1061/(ASCE)0733-9445(2005)131:9(1422).

[13] S. C. Lee, J. Y. Cho, and F. J. Vecchio, “Model for post-yield tension stiffening and rebar rupture in concrete members,” *Eng. Struct.*, vol. 33, no. 5, pp. 1723–1733, 2011, doi: 10.1016/j.engstruct.2011.02.009.

[14] “SAP 2000.” [Online]. Available: www.csiamerica.com/products/sap2000.

[15] “seismostruct.” [Online]. Available: https://seismosoft.com/product/seismostruct/.

[16] H. Q. Wu and Gilbert. R I, “An experimental study of tension stiffening in reinforced concrete members under short-term and long-term loads,” Sydney, 2008.

[17] M. P. Collins and D. Mitchell, *Prestressed concrete structures*. New Jersey: Prentice Hall, 1991.

[18] E. Hernández-Montes and L. M. Gil-Martín, *Hormigón Armado y Pretensado (concreto reforzado y preesforzado)*, 2nd ed. Madrid: Colegio de Ingenieros de Caminos, Canales y Puertos, 2014.

[19] A.-A. C. 445, “Recent Approaches to Shear Design of Structural Concrete: By ASCE-ACI Committee 445 on Shear and Torsion,” *J. Struct. Eng.*, vol. 124, no. 12, pp. 1375–1417, 1998, doi: 10.1061/(ASCE)0733-9445(1998)124:12(1375).

[20] CEB, “CEB Design Manual on Cracking and deformations. 1983. Comité Euro-International du Béton.,” 1983.

[21] L. M. Gil-Martín, E. Hernández-Montes, M. A. Aschheim, and P. Pantazopoulou, “Refinements to compression field theory, with application to wall-type structures,” in *American Concrete Institute, ACI Special Publication*, 2009, no. 265 SP, pp. 123–142.

[22] D. V. Bompa and A. Y. Elghazouli, “Bond-slip response of deformed bars in rubberised concrete,” *Constr. Build. Mater.*, vol. 154, pp. 884–898, 2017, doi: 10.1016/j.conbuildmat.2017.08.016.